



CHORUS

This is the accepted manuscript made available via CHORUS. The article has been published as:

Anomalous Refraction of Acoustic Guided Waves in Solids with Geometrically Tapered Metasurfaces

Hongfei Zhu and Fabio Semperlotti

Phys. Rev. Lett. **117**, 034302 — Published 15 July 2016

DOI: [10.1103/PhysRevLett.117.034302](https://doi.org/10.1103/PhysRevLett.117.034302)

Anomalous refraction of acoustic guided waves in solids with geometrically tapered metasurfaces

Hongfei Zhu^{1,*} and Fabio Semperlotti^{1,2,†}

¹*Department of Aerospace and Mechanical Engineering,
University of Notre Dame, Notre Dame, IN 46556, USA*

²*Ray W. Herrick Laboratories, School of Mechanical Engineering,
Purdue University, West Lafayette, Indiana 47907, USA*

(Dated: June 27, 2016)

The concept of metasurface has recently opened new exciting directions to engineer the refraction properties in both optical and acoustic media. Metasurfaces are typically designed by assembling arrays of sub-wavelength anisotropic scatterers able to mold incoming wavefronts in rather unconventional ways. The concept of metasurface was pioneered in photonics and later extended to acoustics while its application to the propagation of elastic waves in solids is still relatively unexplored. We investigate the design of acoustic metasurfaces to control elastic guided waves in thin-walled structural elements. These engineered discontinuities enable anomalous refraction of guided wave modes according to the generalized Snell's law. The metasurfaces are made out of locally-resonant torus-like tapers enabling accurate phase shift of the incoming wave which ultimately affects the refraction properties. We show that anomalous refraction can be achieved on transmitted antisymmetric modes (A_0) either when using a symmetric (S_0) or antisymmetric (A_0) incident wave, the former clearly involving mode conversion. The same metasurface design also allows achieving structure embedded planar focal lenses and phase masks for non-paraxial propagation.

The concept of metasurface has recently emerged as a powerful approach to effectively manipulate wave-like fields while breaking the dependence on the propagation length. Metasurfaces [1] were first studied in optics and implemented via optical antennas [2, 3] or microwave metamaterials [4, 5] in the context of light propagation across phase discontinuities. The Generalized Snell's Law (GSL) was introduced in order to predict the anomalous propagation across material interfaces characterized by a phase gradient [2]. Optical devices able to achieve unconventional wavefront manipulation capabilities have been theoretically predicted and experimentally demonstrated. A few remarkable examples concern bending light in arbitrary shapes [3, 6], conversion of propagating into surface modes [7], and the development of ultrathin lenses [8, 9]. Shortly after the introduction of metasurfaces in optics, the concept was adopted in acoustics with the intent to create subwavelength acoustic devices. To-date, the most notable design of an acoustic metasurface is based on the labyrinthine [10–14], or space-coiling unit. Anomalous reflection and refraction have been both numerically [15, 16] and experimentally [17–22] demonstrated with labyrinthine units based on phase discontinuities. For completeness, we note that acoustic metasurfaces based on impedance discontinuities (as opposed to phase discontinuities) have also been theoretically demonstrated [23, 24].

Despite much progress in the development of these sub-wavelength designs in both optics and acoustics, the extension of this concept to the control of elastic waves in solids has not received much attention other than for a few studies on elastic waveguides with metamaterial inserts [25–27]. The ability to extend the concept of metasurface to a solid could provide novel and important functionalities for structural acoustic waveguides while dras-

tically expanding their range of application. Applications would range from acoustic lenses for ultrasonic imaging and surgery, to dynamic tailoring of structural components for effective vibration and noise control, to passive energy management for effective harvesting. In this article, we show both numerically and experimentally the possibility to successfully design acoustic metasurfaces fully embedded in structural waveguides and able to reliably achieve anomalous refraction. The metasurface design is based on the use of geometric tapers recently introduced by Zhu [28] in the context of thin-walled acoustic metamaterials. Previous results have shown that a periodic lattice of these geometric inhomogeneities can provide a high level of control of the propagation parameters. At the same time, this design drastically reduces the fabrication complexity of traditional metamaterial systems based on a multi-material approach [29–31].

According to the Generalized Snell's Law (GSL)[2], the direction of anomalous refraction is related to the direction of the incident planar wavefront as follows:

$$\frac{\sin(\theta_t)}{\lambda_t} - \frac{\sin(\theta_i)}{\lambda_i} = \frac{1}{2\pi} \frac{d\phi}{dy} \quad (1)$$

Equation (1) implies that the refracted beam can have an arbitrary direction, provided that a suitable constant phase-gradient ($d\phi/dy$) can be produced along the interface. In order to design metasurfaces that can effectively steer the transmitted guided wave, it is necessary to achieve a spatial gradient profile able to cover the entire 2π phase range. This condition translates into constraints on the frequency response of the different scatterers. In particular, it requires that every scatterer achieves a full 2π phase change while simultaneously maximizing the amplitude of the transmitted wave (i.e. reducing the

back-scattering). Mode conversion is one of the most characteristic traits of acoustic wave propagation in solids as compared to fluids or gases. In the present study, we show the possibility to achieve anomalous refraction for the A_0 anti-symmetric transmitted mode by illuminating the metasurface with either a S_0 or an A_0 incident mode. We will discuss the design for the S_0 excitation in detail while observing that the operating mechanism and the design strategy apply similarly to the A_0 mode.

The proposed approach synthesizes the metasurface based on periodic arrays of elements whose individual unit consists in a geometrically inhomogeneous cell combined with a resonating core. The fundamental building block of the metasurface (Fig.1a) is a square unit (side length $L = 4\text{cm}$) having an embedded elliptic torus-like taper and a (resonating) center mass whose value can be tuned by controlling its thickness. The $x - z$ cross-section of a typical unit is presented in Fig.1b, where t , a , b , r and h are the defining geometric parameters. In this study, we mostly concentrated on the parameter h that is the thickness of the tunable center mass, which affects more directly the local resonance of the building block design, combined with different taper profiles (details provided in Supplementary Material). In order to evaluate the frequency response of the different units, we numerically calculated the transmitted A_0 mode resulting from an incident S_0 plane wave impinging normally on the metasurface. The phase and amplitude response were extracted from displacement data collected in the far-field. The frequency response characterization for each unit was performed on individual 3D strip-like models with a single embedded unit and periodic boundary conditions applied on the top and bottom boundaries, as shown in Fig.1c (top). For the sake of clarity and to facilitate the comparison between different units, we selected a specific frequency of actuation ($f = 20.1\text{ kHz}$) which was used throughout the numerical simulations. This frequency corresponded to a wavelength of the S_0 mode $\lambda_{S_0} \approx 27\text{ cm} \sim 6.75L$ and of the A_0 mode $\lambda_{A_0} \approx 5.9\text{ cm} \sim 1.5L$ for a 8mm thick aluminum plate as considered in the numerical results.

In order to reduce the design complexity while still achieving phase shifts covering the entire 2π range, we recognized that symmetry conditions could be exploited for the S_0 actuation mode. Consider a pair of exactly identical tapered units, a π phase shift difference in the transmitted and mode-converted A_0 wave can be achieved if the units orientation is mirrored with respect to the neutral plane (see Fig.1c); this is a direct result of enforcing the continuity of the displacements in the z direction at the interface between the flat plate and the unit cell. These design considerations were confirmed by the finite element simulations (Fig.1c) that show the out-of-plane displacement field associated with the transmitted A_0 mode. The results of the two models, corresponding to the same taper geometry with mirror symmetry, clearly confirm the phase shift difference of π . Hence,

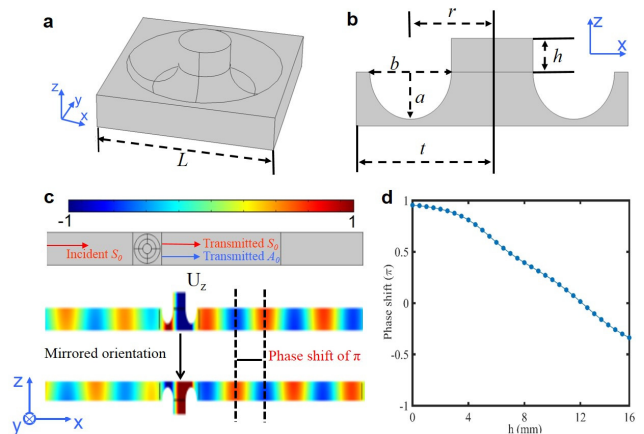


FIG. 1. Schematic of the (a) elliptic torus-like tapered unit and of (b) its xz plane cross-section showing the main geometric parameters. (c) Full field results illustrating the π phase shift occurring on the transmitted (mode converted) A_0 mode generated by a normally incident S_0 mode when the same taper geometry is mirrored about the neutral plane. (d) The phase shift response of a single unit at $f = 20.1\text{ kHz}$ as a function of the thickness of the center mass (which results in a resonance frequency shift).

the use of the mirrored geometry allows reducing the design complexity because the individual units are required to cover only a phase range of π , while the remaining (π) shift can be obtained by a mirroring operation. In fact, the phase shift obtained by varying the thickness h of the attached mass (up to twice the plate thickness) already produces phase shifts largely in excess of π (Fig.1d). These results suggest that a metasurface with a given phase gradient can be designed by carefully selecting unit cells having desired transmission properties (see Fig.1, Supplementary Material).

In the following, we explore the possibility of achieving different wave manipulation effects by exploiting embedded acoustic metasurfaces based on combinations of different fundamental units. In particular, we will show two mechanisms that could prove critical for the development of future ultra-compact acoustic devices: (1) a flat ultra-thin lens, and (2) a phase-mask for non-paraxial propagation.

To illustrate the anomalous refraction phenomenon, which is the fundamental physical mechanism at the basis of all the other designs, we assembled a metasurface based on a one-dimensional periodic array of supercells. The individual supercell was built using different units properly selected to achieve a prescribed spatial phase gradient. The units were fully integrated in the host structure consisting in a 8mm thick aluminum plate, as shown in Fig. 2a. The expected refraction angle $\theta_t = \arcsin\left(\frac{\lambda_t \sin(\theta_i)}{\lambda_i} + \frac{\lambda_t}{2\pi} \frac{d\phi}{dy}\right)$ was predicted according to the GSL. For the numerical investigation, we built a supercell based on different units (see Supplementary Material). The three different configurations provided a phase

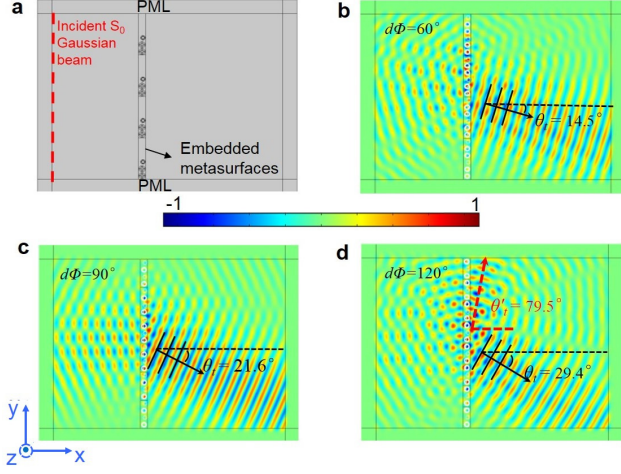


FIG. 2. (a) Schematic of the thin plate with the embedded metasurface. A S_0 Gaussian beam with normal incidence was used as external excitation. Perfectly Matched Layers surrounding the domain of simulation and used to minimize boundary reflections. (b)-(d) shows the transmitted (mode-converted) A_0 wave field for three metasurfaces having different value of the spatial gradient obtained by numerical FEM simulations.

1 shift of $d\phi = \pi/3$, $d\phi = \pi/2$, $d\phi = 2\pi/3$ along the inter-
 2 face. The metasurface was excited by a normally incident
 3 S_0 Gaussian beam from left to right. Figure 2b-c show
 4 the transmitted A_0 mode for the different values of the
 5 phase gradient. Note that, in all the following numerical
 6 results the A_0 wave fields are always plotted in terms of
 7 out-of-plane displacements (z -component) at the neutral
 8 plane of the plate which allows for an effective separation
 9 of the S_0 and A_0 modes. The numerical results for every
 10 configuration show clear evidence of the anomalous
 11 refraction phenomenon. The superimposed black arrows
 12 in Fig. 2b-d indicate the analytical prediction accord-
 13 ing to GSL, that is $\theta_t^{(60^\circ)} \approx 14.5^\circ$, $\theta_t^{(90^\circ)} \approx 21.6^\circ$ and
 14 $\theta_t^{(120^\circ)} \approx 29.4^\circ$. For comparison, the angles of refraction
 15 were also extracted from the full field numerical simula-
 16 tions which provided the following values 15.25° , 22.16° ,
 17 and 28.65° .

18 Only in the case of the strongest spatial gradient
 19 (Fig. 2d), a visible portion of the incident beam was
 20 converted into a second refracted beam. This can be
 21 explained by the existence of a critical value for the
 22 phase discretization, that is the value of $d\phi$ between
 23 adjacent units. It can be shown that, beyond a certain
 24 value of $d\phi$ two possible propagating wave solutions
 25 can be supported by the same metasurface configura-
 26 tion. The refraction angle of the second refracted beam
 27 can be determined by $\theta_t' = \arcsin \frac{\lambda}{2\pi} \frac{-4/3\pi}{dy} = -79.5^\circ$
 28 which is in good agreement with the numerical simula-
 29 tion (dashed red arrow in Fig. 2d). In our current con-
 30 figuration, the critical value for $d\phi$ can be calculated as
 31 $d\phi_c = 2\pi - \frac{2\pi dx}{\lambda} = 0.644\pi$. Aside from these additional

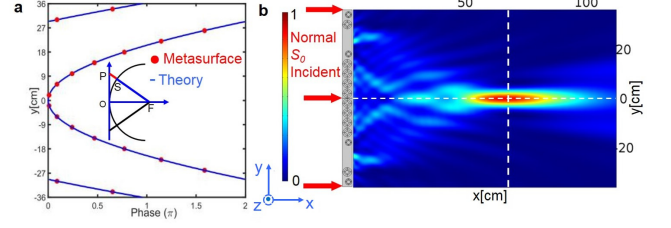


FIG. 3. Design and numerical evaluation of a flat focal lens based on the embedded metasurface concept. (a) shows the continuous hyperbolic phase profile (blue curves) and the corresponding discrete phase profile (red dots) effectively implemented in the metasurface. The inset illustrates schematically how to synthesize the phase profile. (b) The intensity distribution $|A|^2$ of the transmitted A_0 wave field after the flat focal lens.

considerations, results clearly illustrate that the proposed metasurface design is able to induce strong anomalous refraction on the A_0 -converted Lamb modes.

In order to apply this methodology to design a flat focal lens, a hyperbolic phase profile must be programmed into the metasurface (Fig.3a). For a given focal length f , the phase shift $\phi(y)$ profile is provided by:

$$\phi(y) = \vec{k} \cdot \overline{SP} = \frac{2\pi}{\lambda} (\sqrt{f^2 + y^2} - f) \quad (2)$$

where \vec{k} is the wave vector, \overline{SP} is the distance to compensate for in order to achieve a hyperbolic profile, and f is the focal length (that is the distance \overline{OF}).

To show the capabilities of the metasurface, we designed a lens having a focal length $f = 70$ cm. The corresponding phase profile needed to achieve this performance was obtained according to Eqn.2 and plotted in Fig. 3a (blue curve). The corresponding discrete phase profile (red dots) is plotted in Fig. 3a and the lens can be readily constructed by selecting units that match the requested phase shift (see Supplementary Material). Note that the lens was designed with the intent to use a normally incident S_0 excitation and to achieve a focal point in the transmitted A_0 (converted) mode. Figure 3b shows the spatial distribution of the intensity of the transmitted wave field $|A|^2$ after the metasurface. A very narrow focal point is achieved at $x \approx 68$ cm which is within a 3 % error from the target location ($f = 70$ cm). Further analyses about the performance of the acoustic lens can be found in the Supplementary Material.

Our metasurface design can also be exploited to create *phase masks* (essentially, acoustic analog filters) to generate self accelerating acoustic beams that propagate along an arbitrary convex trajectory; a mechanism also known as non-paraxial propagation. We design the metasurface to perform as a phase mask able to convert an incident wave into a non-paraxial beam. Based on the caustic theory [32–34], the continuous phase profile along the metasurface can be synthesized in order to achieve an arbitrary convex trajectory of the transmitted acoustic

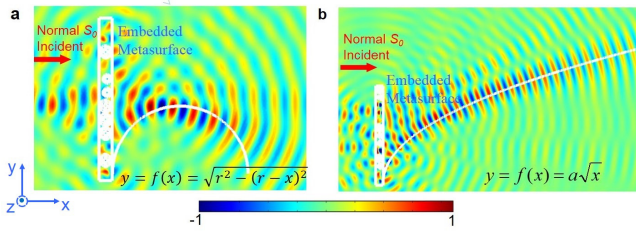


FIG. 4. Non-paraxial self-accelerating acoustic beam achievable by a metasurface phase mask. Numerical simulations illustrated that both designs can successfully achieve non-paraxial beams on the transmitted A_0 mode under normal S_0 excitation for either (a) a half circular trajectory path and (b) a parabolic trajectory. The white solid lines in each plot represent the target trajectory.

1 beam. Once the continuous phase profile is available, its
 2 discrete approximation can be easily obtained by select-
 3 ing basic unit cells according to an analogous procedure
 4 to that described for the flat lens. The detailed descrip-
 5 tion to construct the phase profile $\phi(y_0)$ for an arbitrary
 6 convex trajectory $y = f(x)$ can be found in Supplemen-
 7 tary Material.

8 The ability of the metasurface to generate non-paraxial
 9 beam propagation is numerically shown by means of
 10 two different examples: (1) a half circular and (2) a
 11 parabolic trajectory. The half circular path having ra-
 12 dius r and centered at $(r, 0)$ is described by the equation
 13 $y = f(x) = \sqrt{r^2 - (r - x)^2}$. The desired phase profile is
 14 $\phi(y_0) = -k_0 * (y_0 - 2r * \arctan(y_0/r))$. Concerning the
 15 parabolic trajectory $y = f(x) = a * \sqrt{x}$, the desired phase
 16 profile is $\phi(y_0) = -k_0 * (-\ln(y_0 + \sqrt{y_0^2 + (a^2/4)^2})) * a^2/4$.
 17 For the numerical example, the parameters r and a con-
 18 trolling the curvatures of the paths were selected as
 19 $r = 0.2m$ and $a = \sqrt{0.32}$, in order to guarantee the
 20 smoothness of the discrete phase profile. The resulting
 21 metasurfaces were embedded in the host $8mm$ thick plate
 22 and excited by an incident S_0 plane wave. The numeri-
 23 cal results are provided in Fig. 4a and b in terms of
 24 full displacement fields associated with the transmitted
 25 (mode-converted) A_0 wave. In both cases, results show
 26 good agreements between the target and the calculated
 27 trajectories. Clearly the circular trajectory exhibits a
 28 larger error in the far quarter of the path due to the
 29 finite length of the metasurface.

30 The design approach described above was based on
 31 mode conversion which is a useful but not strictly neces-
 32 sary mechanism to build the metasurface. To substantiate
 33 this statement we explored the design of metasurface
 34 able to operate on non-converted mode that is, as an ex-
 35 ample, on transmitted A_0 modes generated by incident
 36 A_0 modes. The results (summarized in Fig.2 of the sup-
 37 plementary material) showed that comparable anomalous
 38 refraction performance can be achieved also for this al-
 39 ternative design.

40 In order to validate the concept of geometrically tai-

41 lored acoustic metasurface, we performed a set of ex-
 42 perimental investigations. Three different testbeds were
 43 built so to validate the anomalous refraction under 1)
 44 mode converted ($S_0 - A_0$) and 2) direct ($A_0 - A_0$) actu-
 45 ation mode, and 3) the parabolic non-paraxial propaga-
 46 tion. The experimental testbeds consisted of a thin flat
 47 aluminum plate having a single embedded metasurface
 48 (see Fig. 5a; the zoom-in view of the white box shows the
 49 fundamental supercell). The plate thickness was reduced
 50 to 4.06 mm and the target operating frequency was set
 51 to 50.1 kHz. The torus-like tapers were CNC machined
 52 while the center masses were successively glued on the
 53 taper. The experimental sample was mounted in an alu-
 54 minium frame and a viscoelastic tape was glued on the
 55 edges in order to minimize boundary reflections. The
 56 out-of-plane response of the plate was acquired by using
 57 a Polytec PSV-500 laser scanning vibrometer.

58 The full field experimental measurements for the two
 59 anomalous refraction cases are shown in Fig. 5b and
 60 c. An array of Micro Fiber Composite (MFC) patches
 61 (Fig.5a) was surface bonded on the plate and simulta-
 62 neously actuated to generate a quasi A_0 planar incident
 63 wave. Similarly, for the S_0 actuation an identical array of
 64 MFCs was bonded symmetrically on the other side of the
 65 plate and drive in phase. In both cases, the excitation
 66 was a 25-count wave burst with a 50.1 kHz center fre-
 67 quency. For the $A_0 - A_0$ actuation (Fig.5c) the metasur-
 68 face was assembled based on periodic supercells provid-
 69 ing a phase increment of $\frac{2\pi}{3}$ between adjacent units, while
 70 for the $S_0 - A_0$ case (Fig.5b) a phase increment of $\frac{\pi}{2}$ was
 71 used. Note that in these two cases the dimensions of the
 72 subunits are different and correspond to analytical refrac-
 73 tion angles equal to $\theta_t^{S_0-A_0} = \arcsin(\frac{\lambda_t}{2\pi} \frac{\pi/2}{0.016}) = 22.5^\circ$
 74 and $\theta_t^{A_0-A_0} = \arcsin(\frac{\lambda_t}{2\pi} \frac{2\pi/3}{0.02}) = 24.1^\circ$. The experimen-
 75 tally observed angles are 22.8° and 21.6° correspondingly,
 76 which are in good agreement with both the numerical re-
 77 sults and the analytical predictions. The transmittance is
 78 approximately 0.54 for the direct $A_0 - A_0$ actuation mode
 79 (measured by the ratios of the averaged peak value of in-
 80 cident and refracted wave fronts). For the $S_0 - A_0$ mode,
 81 the incident S_0 wave field was not measured but, based
 82 on the numerical simulations, a transmittance (S_0 to A_0)
 83 around 0.528 was estimated. Figure 5d shows the exper-
 84 imental results for the non-paraxial propagation under
 85 $S_0 - A_0$ operating mode. The white solid line represents
 86 the target trajectory (that is $y = f(x) = \sqrt{0.125 * \sqrt{x}}$)
 87 and highlights the good agreement between the analytical
 88 prediction and experimentally generated acoustic beam.
 89 The numerical simulations corresponding to the experi-
 90 mental configurations are provided in Fig.5 of the Sup-
 91 plementary Material.

92 In conclusions, we have presented and experimentally
 93 demonstrated the design of structure-embedded acoustic
 94 metasurfaces which can be exploited to produce a variety
 95 of unconventional wave manipulation effects in structural
 96 waveguides. Numerical and experimental results were in
 97 excellent agreement showing the robustness of the ap-

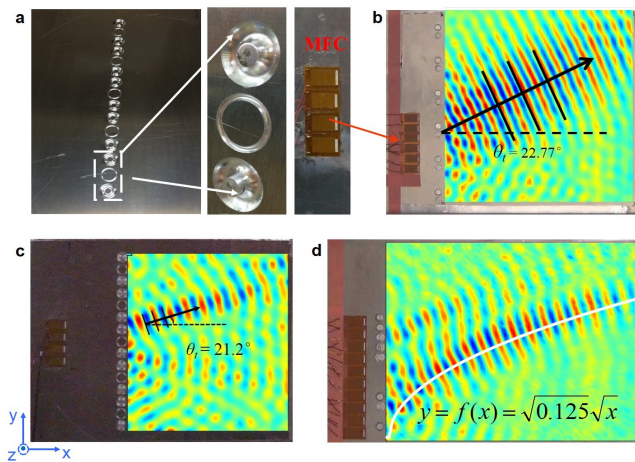


FIG. 5. Experimental setup and results. (a) side view of the embedded metasurface on a 4mm thick aluminum plate. The zoom-in view shows an example of the fundamental supercell from which the metasurface is assembled. An array of MFC pathes was surface bonded to generate the ultrasonic excitation. The measured transmitted A_0 wave fields (out-of-plane component) are shown in (b), (c) and (d) for the $S_0 - A_0$ anomalous refraction, the $A_0 - A_0$ anomalous refraction, and the non-paraxial propagation cases.

proach and the high level of performance achievable with the tapered design. Acoustic wave control was shown for both *same-mode* and *mode-converted* transmitted waves. Applications of the metasurface to acoustic planar focal lenses and phase-masks for non-paraxial propagation were also successfully investigated by numerical simulations and showed an outstanding potential for wave control and device fabrication. The tapers are extremely easy to fabricate and eliminate completely the need for multi-material interfaces typical of the more traditional acoustic metamaterial design. This is a critical aspect to achieve scalability and to transfer metamaterial concepts to structural members with load-bearing capabilities.

The authors gratefully acknowledge the financial support of the Air Force Office of Scientific Research (grant YIP FA9550-15-1-0133) under the supervision of Dr. James Fullerup.

* Hongfei.Zhu.44@nd.edu

† To whom correspondence should be addressed: fsempel@purdue.edu

- [1] N. Yu and F. Capasso, *Nat. Mater.* **13**, 139 (2014).
- [2] N. Yu, P. Genevet, M. A. Kats, F. Aieta, J.-P. Tetienne, F. Capasso, and Z. Gaburro, *Science* **334**, 333 (2011).
- [3] X. Ni, N. K. Emani, A. V. Kildishev, A. Boltasseva, and V. M. Shalaev, *Science* **335**, 427 (2012).
- [4] N. K. Grady, J. E. Heyes, D. R. Chowdhury, Y. Zeng, M. T. Reiten, A. K. Azad, A. J. Taylor, D. A. R. Dalvit, and H.-T. Chen, *Science* **340**, 1304 (2013).

- [5] C. Pfeiffer and A. Grbic, *Phys. Rev. Lett.* **110**, 197401 (2013).
- [6] L. Huang, X. Chen, H. Muhlenbernd, G. Li, B. Bai, Q. Tan, G. Jin, T. Zentgraf, and S. Zhang, *Nano. Lett.* **12**, 5750 (2012).
- [7] S. Sun, Q. He, S. Xiao, Q. Xu, X. Li, and L. Zhou, *Nat. Mater.* **11**, 426 (2012).
- [8] F. Aieta, P. Genevet, M. A. Kats, N. Yu, R. Blanchard, Z. Gaburro, and F. Capasso, *Nano. Lett.* **12**, 4932 (2012).
- [9] M. Kang, T. Feng, H.-T. Wang, and J. Li, *Opt. Express* **20**, 15882 (2012).
- [10] Z. Liang and J. Li, *Phys. Rev. Lett.* **108**, 114301 (2012).
- [11] Y. Li, B. Liang, X. Tao, X.-f. Zhu, X.-y. Zou, and J.-c. Cheng, *Appl. Phys. Lett.* **101** (2012).
- [12] Z. Liang, T. Feng, S. Lok, F. Liu, K. B. Ng, C. H. Chan, J. Wang, S. Han, S. Lee, and J. Li, *Sci. Rep.* **3** (2013).
- [13] Y. Xie, B.-I. Popa, L. Zigoneanu, and S. A. Cummer, *Phys. Rev. Lett.* **110**, 175501 (2013).
- [14] T. Frenzel, J. David Brehm, T. Bckmann, R. Schittny, M. Kadic, and M. Wegener, *Appl. Phys. Lett.* **103** (2013).
- [15] J. Mei and Y. Wu, *New. J. Phys.* **16**, 123007 (2014).
- [16] Y. Li, B. Liang, Z. Gu, X. Zou, and J. Cheng, *Sci. Rep.* **3** (2013).
- [17] Y. Li, X. Jiang, R.-q. Li, B. Liang, X.-y. Zou, L.-l. Yin, and J.-c. Cheng, *Phys. Rev. Applied* **2**, 064002 (2014).
- [18] Y. Xie, W. Wang, H. Chen, A. Konneker, B.-I. Popa, and S. A. Cummer, *Nat. Comm.* **5** (2014).
- [19] K. Tang, C. Qiu, M. Ke, J. Lu, Y. Ye, and Z. Liu, *Sci. Rep.* **4** (2014).
- [20] Y. Zhu, X. Zou, R. Li, X. Jiang, J. Tu, B. Liang, and J.-C. Cheng, *Sci. Rep.* **5** (2015).
- [21] B. Yuan, Y. Cheng, and X. Liu, *Appl. Phys. Express.* **8** (2015).
- [22] K. Tang, C. Qiu, J. Lu, M. Ke, and Z. Liu, *J. Appl. Phys.* **117** (2015).
- [23] J. Zhao, B. Li, Z. Chen, and C. W. Qiu, *Sci. Rep.* **3** (2013).
- [24] J. Zhao, B. Li, Z. N. Chen, and C.-W. Qiu, *Appl. Phys. Lett.* **103** (2013).
- [25] X. Yan, R. Zhu, G. Huang, and F.-G. Yuan, *Appl. Phys. Lett.* **103** (2013).
- [26] R. Zhu, X. Liu, G.K.Hu, C. Sun, and G. Huang, *Nat. Comm.* **5**, 5510 (2014).
- [27] R. Zhu, X. Liu, and G. Huang, *Wave Motion* **55**, 73 (2015).
- [28] H. Zhu and F. Semperlotti, *Phys. Rev. B* **91**, 104304 (2015).
- [29] Y. Wu, Y. Lai, and Z.-Q. Zhang, *Phys. Rev. Lett.* **107**, 105506 (2011).
- [30] Y. Lai, Y. Wu, P. Sheng, and Z.-Q. Zhang, *Nat. Mat.* **10**, 620 (2011).
- [31] X. N. Liu, G. K. Hu, G. L. Huang, and C. T. Sun, *Appl. Phys. Lett.* **98** (2011).
- [32] E. Greenfield, M. Segev, W. Walasik, and O. Raz, *Phys. Rev. Lett.* **106**, 213902 (2011).
- [33] S. Zhao, Y. Hu, J. Lu, X. Qiu, J. Cheng, and I. Burnett, *Sci. Rep.* **4** (2014).
- [34] L. Froehly, F. Courvoisier, A. Mathis, M. Jacquot, L. Furfaro, R. Giust, P. A. Lacourt, and J. M. Dudley, *Opt. Express* **19**, 16455 (2011).